GEOPERSIA

Accepted Manuscript

Influence of Active Tectonics on Drainage Geomorphic Evolution of the Rit Anticline, Zagros Fold-and-Thrust Belt

Somaye Derikvand, Fatane Rokrok

DOI: 10.22059/geope.2026.407702.648853

Receive Date: 06 December 2025
Revise Date: 04 June 2026
Accept Date: 13 July 2026

Influence of Active Tectonics on Drainage Geomorphic Evolution of the Rit Anticline, Zagros Fold-and-Thrust Belt

Somaye Derikvand *, **Fatane Rokrok**

College of Sciences, Lorestan University, Khoramabad, 68148, Iran

Received: 06 December 2025, Revised: 04 June 2026, Accepted: 13 July 2026

Abstract

This study investigates the influence of active tectonics on the drainage patterns and geomorphic characteristics of the Rit Anticline, located within the Simply Folded Belt of the Zagros fold-and-thrust belt. Morphometric analysis was conducted for 93 drainage basins using six basin-scale indices — AF, HI, Bs, CI, Smd, and SL — together with drainage-network parameters including Dd, Dd1, Df, N1/N, and Sd. One-way ANOVA and pairwise Welch t-tests identified significant among-sector variation in four parameters: HI ($F = 5.946$, $p = 0.003$), CI ($F = 3.178$, $p = 0.046$), Smd ($F = 3.125$, $p = 0.048$), and SL ($F = 3.021$, $p = 0.036$), while AF and Bs showed no significant variation, reflecting the structural coherence of the anticline as a continuous fold. The western sector is morphometrically the most distinct, showing significantly higher CI (1.54 vs. 1.18, $p = 0.032$) and HI (0.500 vs. 0.488, $p = 0.009$) relative to the central sector, significantly lower SL (317.5 vs. 441.5, $p = 0.028$) relative to the central sector, and significantly higher Smd (1.19 vs. 1.1, $p = 0.007$) relative to the eastern sector, consistent with more advanced lateral fold propagation in this zone. The central sector as the most structurally mature part of the fold has experienced greater structural relief and differential erosional exposure than the propagating terminations. The absence of significant differentiation between the central and eastern sectors supports the interpretation that lateral propagation to the east remains in an earlier stage of development. A strong negative correlation between Bs and CI ($r = -0.411$, $p < 0.01$) suggests geometric compensation between basin elongation and crescent-shaped deformation driven by differential fold curvature. Overall, the results demonstrate that the Rit Anticline is characterized by asymmetric bilateral lateral propagation, more advanced to the west than to the east, governed by the interplay of fault-related folding, transverse–shear faulting, and spatially variable lithologic resistance.

Keywords: Tectonic Geomorphological Indices, Rit Anticline, Fold-And-Thrust Belt, Geomorphic Features, Neotectonics.

Introduction

Active deformation within fold-and-thrust belts is capable of generating major seismic events, posing considerable hazards to surrounding regions (Hubbard & Shaw, 2009; Xu et al., 2009; Lu et al., 2017). Orogenic belts undergoing uplift display distinctive geomorphic signatures produced through the interaction of internal tectonic forces and surface processes. As folds and thrusts grow, they displace stratigraphic units and modify topography, exerting strong control over drainage organization and slope evolution (e.g., Bufe et al., 2016; Bahrami et al., 2020). Consequently, identifying active structural elements, assessing seismic risk, and interpreting river diversions, sediment dynamics, erosion, and landscape evolution are integral components of morphotectonic research and crucial for hazard-management strategies.

Within the Zagros belt-particularly in the simply folded zone–the uplift of structural-domain anticlines has produced a range of tectonically influenced landforms. Quantitative analysis of

* Corresponding author e-mail: derikvand.so@lu.ac.ir

these features provides essential constraints on the style and degree of tectonic deformation. Numerous geomorphic indices have been proposed and applied globally to detect active displacement (Hack, 1973; Wells et al., 1988; Cox, 1994; Keller & Pinter, 2002; El-Hamdouni et al., 2008; Delcaillau et al., 2006). Evaluating fold-growth geometry and the erosional behavior of stream channels offers insight into hinge development during folding (Ahmadi et al., 2006). Advances in GIS, DEM datasets, and satellite-based observations have significantly improved the capacity to conduct morphotectonic analyses in recent years (Singh & Jain, 2009; Font et al., 2010).

Hydro-geomorphic indicators such as drainage density and frequency, bifurcation ratios, and junction angles have been widely investigated in relation to active tectonics (Talling & Sowter, 1999; Jamieson et al., 2004). Drainage anomalies and pattern variations can preserve evidence of ongoing deformation and fold growth (Deffontaines et al., 1992; Delcaillau et al., 2006; Simoni et al., 2003; Ramasamy et al., 2011). More recently, several studies have underscored the diagnostic value of drainage-system characteristics for recognizing neotectonic activity. For example, Ramsey et al. (2008) showed that asymmetric tributary arrangements and the alignment of stream heads parallel to anticline crests constitute robust geomorphic indicators of lateral fold propagation in the Zagros Mountains.

In the Zagros Mountains, numerous studies have been conducted to investigate tectonic activity and analyze morphotectonic characteristics. The results of these studies generally emphasize the active role of tectonic structures in the evolution of landforms and drainage networks. In this regard, Yamani and Sharafi (2011) analyzed morphological changes of the Harroud River in Lorestan and demonstrated the role of tectonics in river displacement and channel migration. Faghih et al. (2015) assessed active tectonics of the Herang anticline using morphometric and geomorphological indices. Servati et al. (2018) also, by applying geomorphic indices in the Kabirkuh anticline of Ilam, identified moderate to high neotectonic activity in the region. Bahrami (2013), through the analysis of drainage network anomalies in Zagros basins, showed a direct relationship between drainage patterns, tectonic activity intensity, and fold growth. Bahrami et al. (2020) confirmed lateral growth of the Gorm anticline and its influence on drainage network organization using morphometric indices. Bahrami (2022) analyzed the drainage confluence angle in 23 basins of the Zagros Simply Folded Belt and investigated its relationship with morphometric indices, demonstrating its control by fold growth, anticline axes, and fault structures. Alipoor et al. (2019) evaluated relative tectonic activity in the Garin Mountains (near the Nahavand fault) using geomorphic indices and drainage network analysis. Derikvand and Farahpour (2020), using morphometric indices and fractal analysis in the Khorramrud Basin of Lorestan, indicated significant tectonic activity in parts of the region. Ashtraba et al. (2019) confirmed evidence of active tectonics along a major young fault zone in Sarvabad using quantitative and qualitative methods. Ramezani et al. (2023) investigated the role of faults in morphological changes in the Biston–Kamiaran region. Derikvand (2023), using geomorphic indices in northern Pol-e Dokhtar, identified moderate to very high tectonic activity in sub-basins. Maleki et al. (2024) in southwest Ilam and Mirahadi et al. (2024) in northwest Sahneh also confirmed active tectonic structures and their role in landform evolution using morphometric indices.

Overall, these studies demonstrate that morphometric and morphotectonic indices are effective and reliable tools for evaluating tectonic activity and analyzing geomorphological evolution, particularly in the active Zagros belt. Since the relationship between active tectonics and geomorphology in the Rit anticline basin has not yet been thoroughly investigated, morphometric analysis is considered essential for identifying the influence of active tectonics on drainage basin evolution and the lateral growth of this anticline. The present study aims to assess tectonic activity within the watershed of the Rit anticline, situated in the fold-and-thrust segment of the Zagros range in southern Lorestan Province, a region characterized by elongated and continuous mountain ridges. To achieve this, a combination of geomorphic and structural analyses was applied using ArcGIS-based methods and digital topographic data from the Shuttle Radar Topography Mission (SRTM), supplemented by prior research and expert geological interpretations.

This paper focuses on evaluating basin morphometry and drainage-network characteristics to infer active tectonics and lateral fold growth of the Rit anticline within the broader Zagros fold belt. For this purpose, a suite of geomorphic parameters was examined, including the asymmetry factor (AF), hypsometric integral (HI), basin shape index (Bs), crescentness index (CI), main drainage sinuosity (Smd), stream length-gradient index (SL), anticline-crest sinuosity (Sd), stream frequency (Df), drainage density (Dd), and the ratio of first-order channels to total streams (N1/N).

Study area

Geological features

The Rit anticline occupies a position within the central part of the Zagros fold-and-thrust belt, a NW–SE-trending mountain system extending across southwestern Iran. This orogenic belt spans nearly 1,800 km-from the Taurus Mountains in northern Turkey to the Strait of Hormuz in southern Iran (Alavi, 1994). Its development is attributed to the Tertiary collision between the Arabian and Eurasian plates (Agard et al., 2005), which produced approximately 30–32% crustal shortening across the region (Bahroudi & Koyi, 2003). Contemporary seismic and geodetic observations show that the Arabian plate continues to move north–northeastward toward Eurasia at a velocity of roughly 25–30 mm/yr (Talebian & Jackson, 2002; McClusky et al., 2003). The convergence vector intersects the central Zagros at an oblique angle of nearly 50° along the NW–SE structural trend (McClay et al., 2004), contributing to the formation and ongoing activity of folds, thrusts, and strike-slip faults of varying scales (Sarkarinejad & Goftari, 2019). These tectonic interactions govern the morphotectonic character of the region, influencing landscape evolution, structural architecture, seismicity patterns, and fault activity throughout the belt (Agard et al., 2011).

The Zagros foreland is subdivided into several tectono-stratigraphic provinces (Fig. 1a): the Lorestan domain in the west, the Dezful and Izeh embayment in the central sector, and the Fars domain in the east (Falcon, 1974). The Lorestan region contains numerous anticlines composed primarily of Mesozoic–Neogene carbonate successions, among which the Rit fault-related anticline is situated. Its axial trace follows a NW–SE trend, consistent with the dominant structural grain of the Zagros.

Geological exposures within the Rit anticline span from the Middle Cretaceous to the Miocene, while younger Miocene–Quaternary formations occupy valley floors. The Bangestan Group represents the oldest unit and consists of thick carbonate packages interlayered with shale and sandstone. Above it, the Gurpi Formation comprises shale, marl, and marly limestone (Motiei, 1993). The frontal ridge is largely formed by the marly limestones of the Pabdeh Formation, which exhibit lateral transitions into the Amiran Formation (sandstone and siltstone), the Talezang Formation (limestone), and the Kashkan flysch deposits. The Asmari-Shahbazan Formation—dominated by limestone—forms the most extensive outcrops across the anticline. Overlying these units are the Gachsaran Formation (anhydrite, halite, marl, and limestone) and the Aghajari Formation (sandstone, marl, siltstone, and gypsum), representing the youngest lithologies in the area. Figure 2a illustrates the geological map of the region, and Figure 2b shows a cross-section (AA') perpendicular to the Rit anticline.

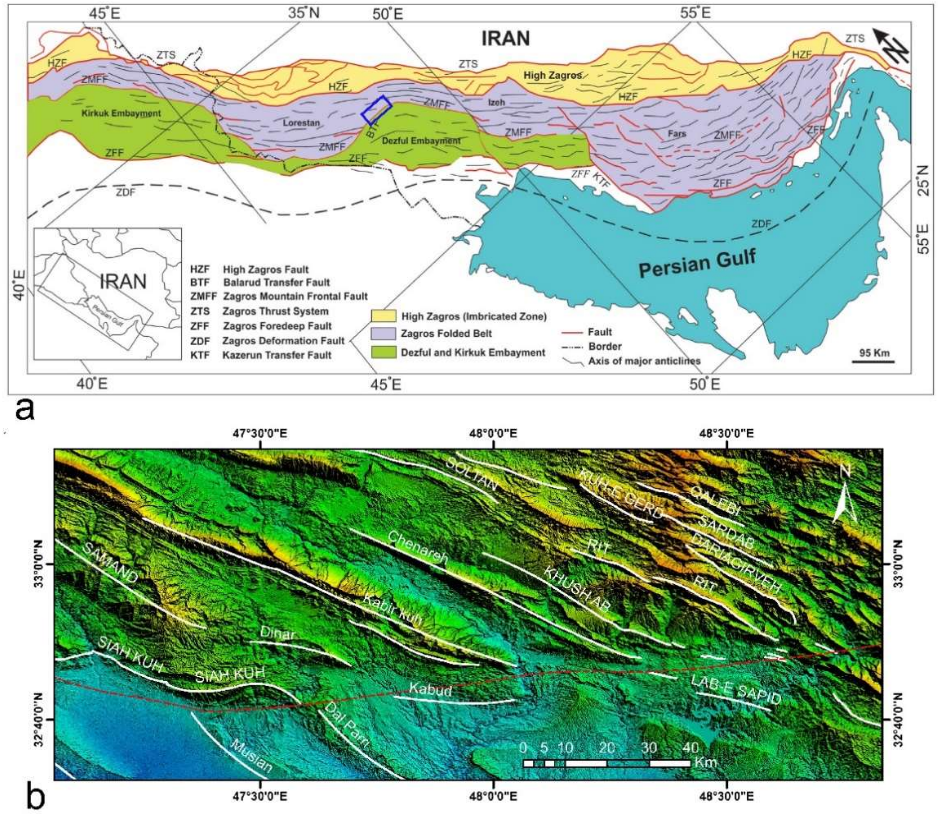

Figure 1. (a) The geological structure and tectonic subdivisions of the Zagros fold-and-thrust belt in southwestern Iran and northeastern Iraq. Solid and folded lines represent the major faults and axes of large folds within the foreland of the Zagros Mountains (Ghanadian et al., 2017). The location shown in Figure b is indicated by a blue rectangle on the map. (b) SRTM topography of the area across the Balarud Fault in the southern part of Lorestan Province. The anticlines near the Balarud Fault trend in an east–west direction. White lines indicate the location of the anticline axes, while the red line shows the position of the subsurface Balarud Fault

Tectonic-geomorphic features

The stratigraphic and tectonic characteristics govern the physical properties of the Zagros orogenic belt. The pattern of drainage networks is closely associated with the evolution of fold-and-thrust structures and the erosion of exposed formations. Owing to strain partitioning between the Zagros folded–thrust belt and the recent major strike-slip fault in the northwest of the region (Talebian & Jackson, 2002), the direction of regional plate convergence is approximately N–S (e.g., Vernant et al., 2004). The Balarud Fault (BRF), as a segment of the Mountain Front Fault (MFF), marks the boundary between the Dezful Embayment and the Lorestan Zone (Fig. 1b).

The Balarud Fault plays a key role in deflecting the fold axes on both sides of the fault zone (Allen & Talebian, 2011). Although the Balarud basement fault does not crop out at the surface, it strongly influences the deformation style of the overlying sedimentary units within the study area (Razavi Pash et al., 2021). The fault exhibits left-lateral strike-slip displacement with a reverse component. Its trend shifts from an E–W orientation to NW–SE in the vicinity of the Rit anticline. This geometric change causes bending of the anticline axis and results in a step-like structural configuration within the Rit fold.

During progressive deformation, multiple detachment horizons and their associated thrust faults have shaped the geometry of the thrust-related folds. Figure 3 shows the thrust fault linked to the Rit anticline within the Bangestan Group, which forms the core of the structure. This fault is exposed at the surface with a NW–SE orientation and, in several locations, has produced changes in bedding dip (Fig. 5g) and even localized overturning of the strata. The thrust-related folding developed within the hanging wall of the fault.

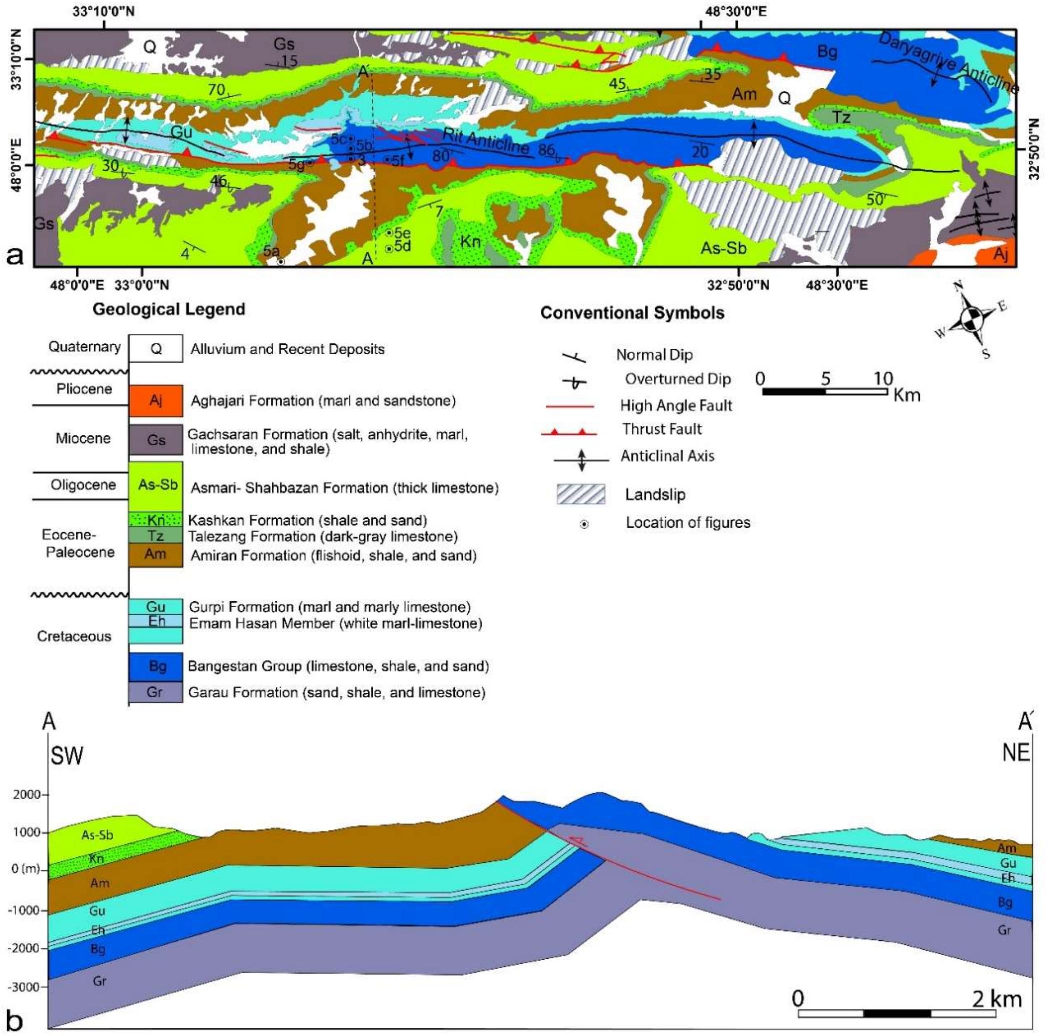

Figure 2. (a) Geological map of the study area at a scale of 1:100,000 (published by the National Iranian Oil Company), showing the location of the cross-section AA′. (b) Cross-section AA′, which transects the anticline and trends northeast–southwest (constructed based on the structural geological map)

Figure 3. Thrust faults associated with the folding of the Rit anticline within the Bangestan Group. The thrust faults are indicated by red lines

The Rit anticline exhibits a box-shaped fold geometry due to its whale-back morphology. Differences in topographic slopes across the eastern, western, and central sectors indicate that it is a doubly plunging, asymmetric fold. Based on these variations, the anticline is divided into three tectonic domains: eastern, central, and western (Fig. 4).

In the study area, the Zal and Damdam rivers flow through highly sinuous channels. Figure 5a provides a clear view of a deep valley and a river incising through the resistant layers of the Asmari Formation. The valley walls consist of nearly regular and successive bedding surfaces with gentle to sub-horizontal dips. This type of incision indicates active tectonic uplift, which has forced the river to abandon its meandering pattern on the plain and enter a phase of active vertical erosion. The deeply incised V-shaped valley morphology is a clear indicator of erosional response to tectonic activity. The narrow and deeply entrenched valleys (Figs. 5b, c, d), located near the mountain front, represent gorges that serve as additional evidence of ongoing tectonic activity. Some of these valleys host active watercourses, whereas others are dry. The presence of deep fluvial incisions, fault-generated scarps, and knickpoints (Fig. 5e) collectively reflects the active tectonic regime of the region.

The interaction between tectonic activity and erosional processes within the anticline, together with the dissection of the drainage network, has resulted in the development of steep triangular facets along the Rit anticline (Figs. 5f, 5g, and 6). These triangular facets, typically observed along valley margins and adjacent to active faults, represent structural boundaries formed by vertical fault movements. They are essentially remnants of recent fault activity, commonly displaying a broad base at the bottom and a sharp apex at the top. The spatial distribution of these facets in geomorphologically active zones-particularly along faulted slopes-indicates youthful topography and dynamic tectonic uplift. Wine-glass–shaped valleys have formed through the erosion of these triangular facets (Fig. 6). These landforms provide strong evidence of recent uplift in the study area. They are characterized by a wide, open upper valley and a narrow, focused lower segment, reflecting concentrated erosion at the base of fault scarps. Such forms typically develop at active knickpoints or in areas with pronounced elevation drops and are reliable geomorphic indicators of recent tectonic activity (Burbank and Anderson, 2011).

In the eastern sector of the anticline, the presence of fractures and deep valleys arranged in a radial pattern reveals active faulting and uplift. The transverse incision of the anticline by the Damdam River demonstrates fluvial erosion occurring concurrently with tectonic uplift. The steep mountain front, accompanied by radial incisions and triangular facets, highlights the high rate of uplift and the disequilibrium between erosion and uplift. The occurrence of alluvial fans downstream of the slopes suggests rapid sedimentation in response to slope instability. A landslide has occurred on the southern limb of the anticline as a result of tectonic activity (Fig. 6).

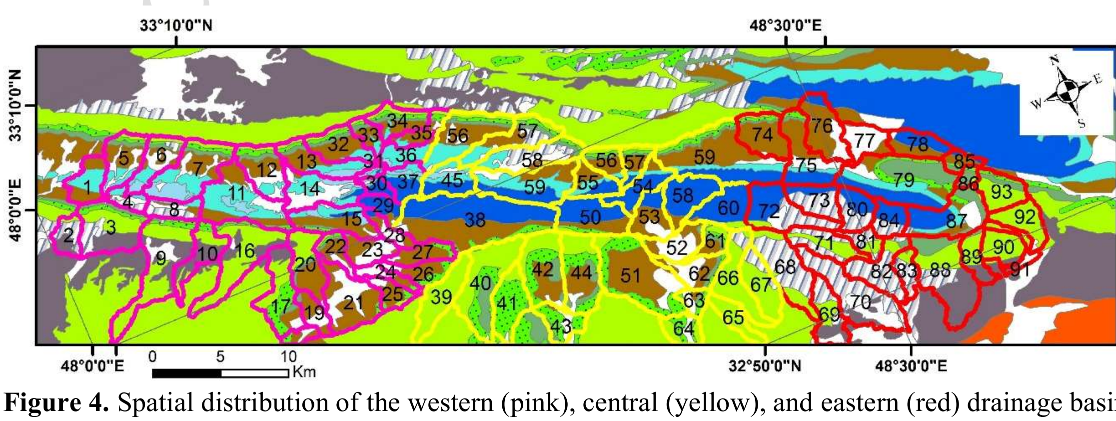

Figure 4. Spatial distribution of the western (pink), central (yellow), and eastern (red) drainage basins of the Rit Anticline overlaid on the geological map of the study area

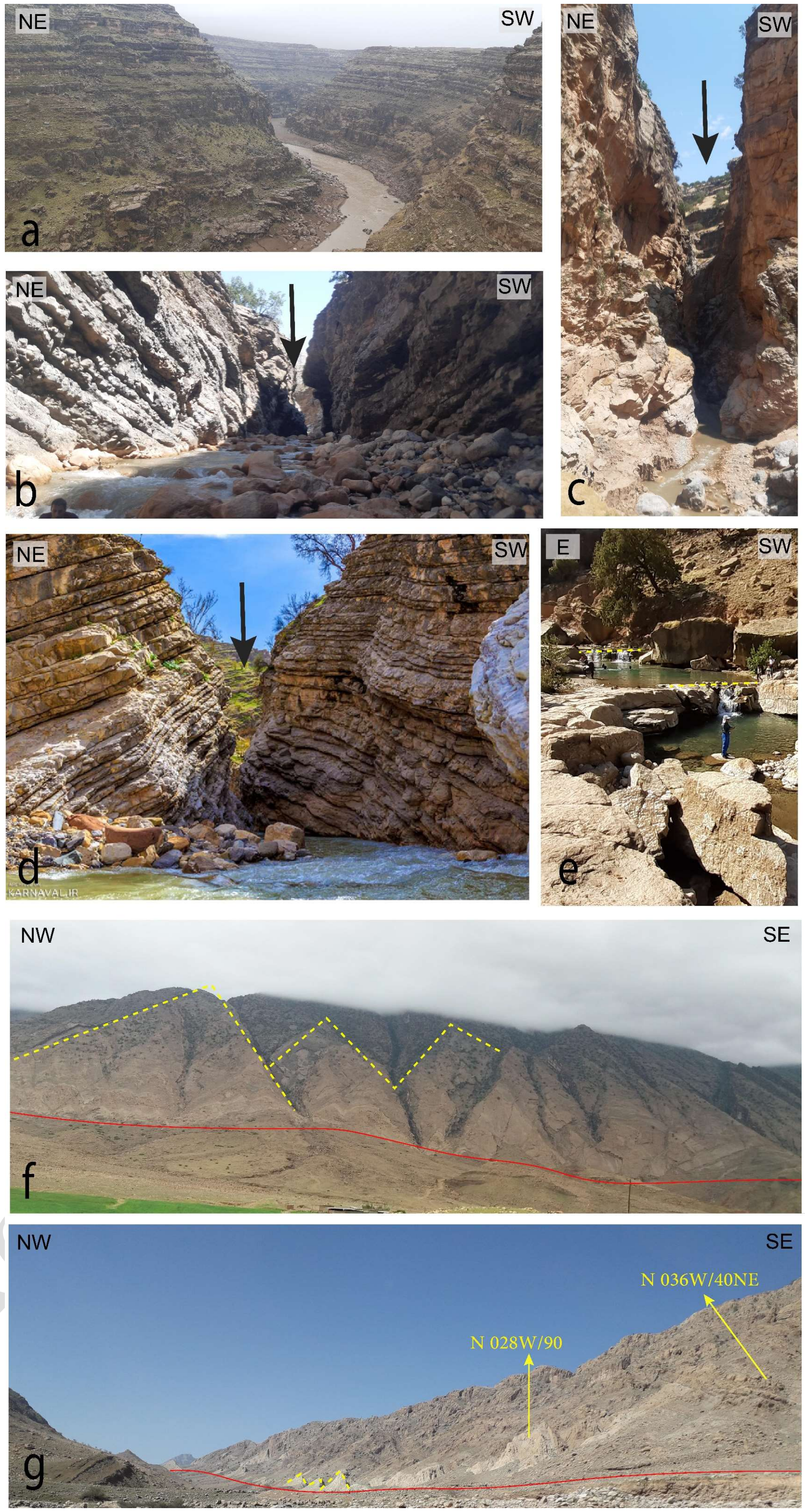

Figure 5. (a) Meandering channel of the Zal River cutting through the Asmari-Shahbazan Formation. (b, c) Narrow and deep gorges located within the Helt Gorge. (d) Deep and narrow gorge in the Kul Chap area. (e) Fault scarps forming knickpoints along the Helt Gorge. (f) Triangular facets developed along the thrust fault associated with the Rit anticline. (g) Triangular facets at the thrust fault of the anticline, showing layer slope changes caused by fault activity

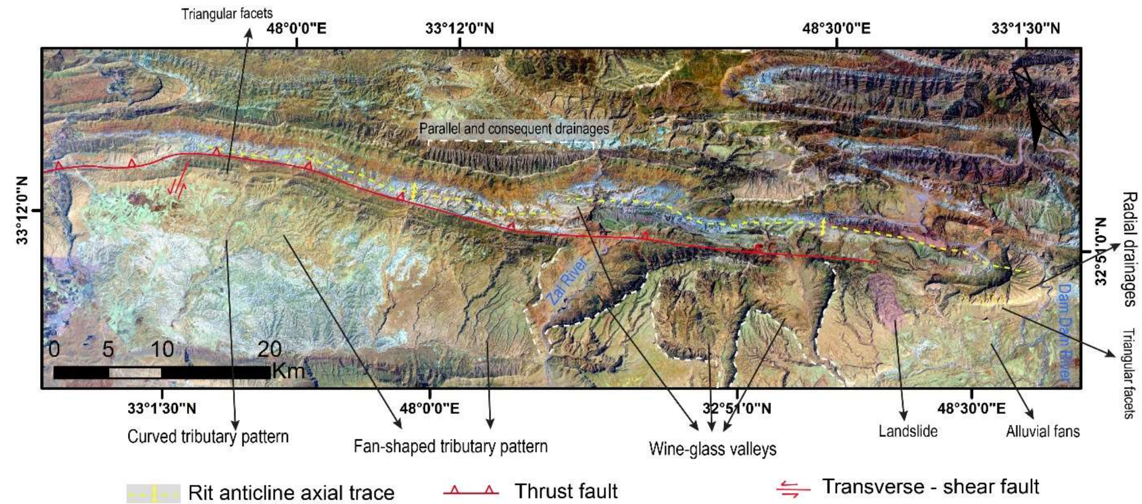

Figure 6. Landsat satellite image of the Rit anticline acquired by the OLI sensor. The image was processed in ArcGIS using a combination of bands 4, 7, and 1

In the central sector of the anticline, the fold axis appears continuous with a gentle curvature. The presence of gorges and deep fluvial incisions along the fold axis indicates the interplay between tectonic uplift and river incision. The Zal River has maintained its course by cutting through resistant formations. Fan-shaped drainage networks extend from the southern flank of the anticline toward the surrounding plains. These patterns reflect the influence of active faults and scarp boundaries, with youthful, incompletely developed channels forming in response to structural uplift. In addition, the presence of incision and summit erosion along the fold crest points to the ongoing influence of neotectonic forces in the central sector. Three wine-glass–shaped valleys are observed in the footwall of the thrust fault associated with the Rit anticline. Their occurrence at the intersections of channels with structural fractures confirms the direct role of neotectonics in their formation (Fig. 6). The activity of young faults may ease the flow of water and enhance the rate of headward erosion (Koshnaw et al., 2024).

In the western sector of the anticline, the interaction between fracture systems and folding has produced incisions and deflected channels along the valleys. The presence of transverse valleys relative to the anticline axis indicates river erosion taking place alongside active uplift. Multiple erosional surfaces, dissected mountain fronts, triangular facets, curved channel patterns, parallel drainage, and fan-shaped drainage systems collectively point to sustained neotectonic processes in this area. The parallel drainage paths have developed under the influence of transverse fractures associated with the anticline. A transverse-shear fault with left-lateral motion has displaced the bedding and produced bending along the anticline axis (Fig. 6).

Materials and methods

To assess the lateral propagation of the Rit anticline, ALOS DEM data with a spatial resolution of 12.5 meters were employed for integrated morphometric analyses and geomorphic interpretation. Stream orders and lengths were determined, and the drainage network of the study area was generated using the Hydrology toolbox in ArcGIS (Fig. 8f). Through the combined use of Google Earth™ imagery and ALOS DEM datasets, a total of 93 drainage basins were mapped across the Rit anticline. Basin centerlines were calculated using the distance analysis module in ILWIS. Lithological information was obtained from 1:100,000-scale geological maps.

The mechanical strength of bedrock plays a crucial role in shaping drainage morphology, network geometry, and associated landforms (Stokes & Mather, 2015). Variations in lithological resistance can modify basin morphometry and influence drainage organization. Considering the significance of rock strength in morphometric development (Stokes & Mather, 2015), the lithostratigraphic units of the study area were classified into three general strength categories following earlier studies (Sepehr & Honarmandnejad, 2012; Pirouvan & Shariat Jafari, 2013):

Category 1 – High resistance: Bangestan Group, and the Talezang and Asmari Formations.

Category 2 – Intermediate resistance: Gurpi, Amiran, Pabdeh, Kashkan, and Gachsaran Formations.

Category 3 – Low resistance: Quaternary terraces and alluvial deposits.

In total, 39%, 43%, and 18% of the study area are underlain by high-, medium-, and low-strength rock units, respectively (Fig. 7).

Six morphometric indices and five drainage system parameters were calculated to characterize basin geometry and evaluate tectonic activity along the anticline. Each index was extracted from the ALOS DEM or derived drainage network, and interpreted in the context of fold propagation dynamics, as described below.

Asymmetry factor (AF) is widely applied as an indicator of tectonic tilting at the drainage-basin scale (Keller & Pinter, 2002) and was calculated as:

$$AF = (A_r/A_t) \times 100$$

where *Ar* is the basin area on the right-hand side of the downstream flow direction and *At* is the total basin area. Values deviating significantly from 50 indicate lithologic control, differential erosion, or active tectonics, whereas values close to 50 reflect tectonic stability or the absence of cross-basin tilting (Pérez-Peña et al., 2010). To facilitate comparison of tilting intensity irrespective of tilt direction, the absolute deviation from the equilibrium value was used in the analysis and reported as $|AF - 50|$. Therefore, values close to zero indicate near-symmetric basins, whereas larger values reflect increasing basin asymmetry and stronger tectonic tilting. AF was computed for all 93 basins using the drainage network and basin polygons delineated in ArcGIS.

Hypsometric integral (HI) serves as a key geomorphic metric for interpreting the evolutionary stage of drainage basins (Strahler, 1952). The hypsometric curve conveys the geomorphic character of a landscape and reflects the combined influence of climate, lithology, and tectonic deformation on landform development. HI corresponds to the area beneath the normalized hypsometric curve. Hypsometric curves were generated from the ALOS DEM, and a second-order polynomial was fitted to each normalized curve following Liffner (2018); HI was obtained by analytically integrating the fitted function over the normalized elevation range (0–1). Low HI values indicate more mature, extensively eroded landscapes with limited recent uplift (He et al., 2019).

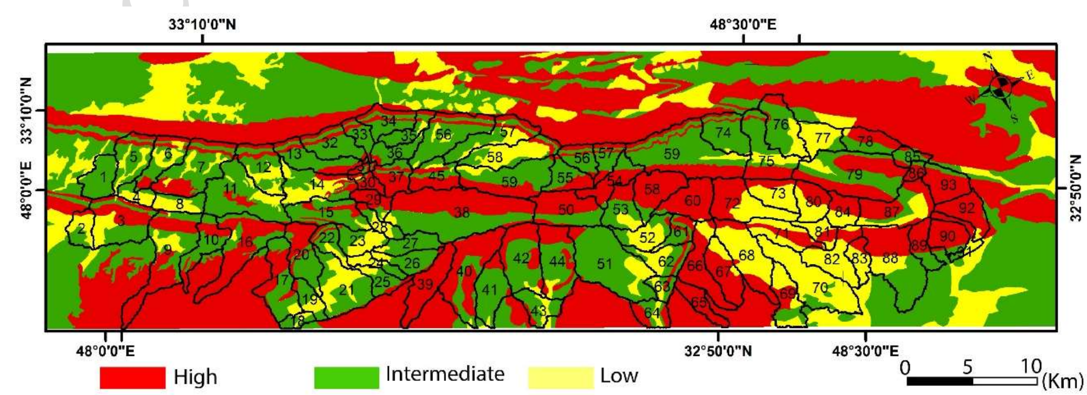

Figure 7. Zonation map of the study area based on rock strength, classified into three groups: strong, medium, and weak

Basin shape index (Bs) quantifies basin elongation and is defined as:

$$Bs = Bl/Bw$$

where *Bl* is the basin midline length and *Bw* is the maximum basin width (Ramírez-Herrera, 1998). Basin midline lengths were extracted using the distance analysis module in ILWIS, and maximum widths were measured from basin polygons. In tectonically active regions, basins tend to develop elongated forms (higher Bs), whereas reduced tectonic influence promotes more circular geometries (Ramkumar et al., 2019). With progressive fold amplification, lateral basin expansion generally results in lower Bs values (Bahrami et al., 2020).

Crescentness index (CI) relates basin geometry to the vertical and lateral growth of anticlines (Bahrami et al., 2020) and is expressed as:

$$CI = LBM/Sl$$

where *LBM* is the basin midline length and *Sl* is the straight-line distance between the two endpoints of the midline. Both parameters were derived from basin centerlines computed in ILWIS. Values approaching 1 indicate straighter basins, while values of 1.5 and above characterize strongly curved, crescent-shaped basins. Higher CI values in basins positioned on fold limbs reflect lateral fold propagation.

Main drainage sinuosity (Smd) is the ratio of the main channel length (*Mc*) to the straight-line distance between its endpoints (*Sl*), and was extracted from the delineated drainage network. Channel sinuosity is influenced by stream gradient and uplift history: older channel segments that have experienced prolonged uplift typically display greater sinuosity than younger segments near actively uplifting fold tips (Bahrami & Stokes, 2023). Accordingly, fold limbs with longer uplift histories yield higher Smd values, while recently uplifted fold noses exhibit lower sinuosity due to insufficient time for meander development.

The stream length-gradient index (SL) was used to evaluate the influence of tectonic activity and lithologic resistance on river longitudinal profiles. This index explains the response of stream longitudinal profiles to environmental changes and is calculated as (Hack, 1973):

$$SL = \left(\frac{\Delta H}{\Delta L}\right) L_t$$

where ΔH is the elevation difference between two points along the stream, ΔL is the horizontal distance between those points, and Lt is the total channel length measured from the midpoint of the analyzed segment to the drainage divide. The SL index is influenced by channel slope, lithologic resistance, topography, and stream length (Zovoili et al., 2004). High SL values are commonly observed in areas where streams incise resistant rock units or where tectonic uplift has increased channel steepness. Because this index is highly sensitive to variations in channel gradient, it can identify irregularities in river longitudinal profiles and reveal the relationship between tectonic deformation, rock resistance, and topographic adjustment (Keller & Pinter, 2002). In regions where a long period has elapsed since the last tectonic activity, variations in SL values may become less pronounced due to progressive erosion and landscape adjustment. The SL index was calculated using longitudinal stream profiles generated from the DEM-derived drainage network in ArcGIS.

Sinuosity of the anticline divide (Sd) is defined as:

$$Sd = LD/LH$$

where *LD* is the total length of the principal anticline divide and *LH* is the length of the hinge line (Bahrami et al., 2020). Both were digitized from the DEM and geological maps. Lower Sd values characterize younger, less eroded portions of the fold—commonly the nose areas-whereas higher values are associated with older, more deeply eroded segments of the anticline core.

In addition to the geometric indices above, drainage frequency (Df), drainage density (Dd), and the ratio of first-order streams (N_1/N) were computed for the main drainage systems in the study area. These parameters relate to multiple environmental and tectonic factors, including vegetation cover, climatic conditions, surface slope, tectonic uplift, and lithology (Keller & Pinter, 2002; Bahrami, 2022), and provide insights into the rate of lateral fold growth and uplift (Azor et al., 2002; Melosh & Keller, 2013; Bahrami & Stokes, 2023). Drainage frequency represents the total number of streams of all orders per unit area, whereas drainage density is defined as the cumulative length of all stream segments divided by basin area (Horton, 1932). Among all drainage orders, first-order channels are the most sensitive indicators of active tectonics (Keller & Pinter, 2002); consequently, anticlines undergoing lateral propagation typically exhibit higher N_1/N ratios. The parameter Dd_1, expressing the ratio of total first-order stream length to basin area, was also calculated to further characterize tectonic sensitivity across the study basins.

Results

Based on the morphometric analyses carried out for the study area, a total of 93 drainage basins were identified across the Rit Anticline. From a tectonic perspective, the anticline is subdivided into three NW–SE–trending sectors—western, central, and eastern—as well as two north–south–oriented flanks, referred to as the northern and southern domains. The mean values of the morphometric indicators—including AF, HI, Bs, CI, Smd, and SL—together with the drainage-network parameters such as Dd, Dd1, Df, N1/N, and Sd, are summarized in Table 1.

Using the calculated AF, HI, Bs, CI, Smd, and SL values, the drainage basins were classified into three tectonic-activity classes: Class 1 (high activity), Class 2 (moderate activity), and Class 3 (low activity), following the criteria proposed by El-Hamdouni et al. (2008) and Bahrami et al. (2024). These indices were then integrated to produce a tectonic-activity zonation map for the region, shown in Figure 8.

The drainage basins vary in size from 1.2 km² (basin 18 in the western sector) to 30.42 km² (basin 38 in the central sector), with the largest basins occurring predominantly in the central region. HI reaches its minimum value of 0.41 in basin 54 (central sector) and its maximum of 0.49 in basin 63 (central sector). AF ranges from a minimum of 0.17 in basin 83 (eastern sector) to a maximum of 33.21 in basin 44 (central sector). Bs shows its lowest value of 0.22 in basin 28 (western sector) and its highest value of 4.21 in basin 66 (central sector). For CI, the minimum value is 0.74 in basin 54 (central) and the maximum is 4.98 in basin 28 (western). SL ranges from a minimum value of 26.72 (western sector) to a maximum value of 2590.27 (western sector), indicating substantial spatial variations in channel gradient, lithologic resistance, and tectonic influence across the study area. Smd is as low as 1 in several eastern basins and reaches a maximum of 1.59 in basin 59 (central sector).

Table 1. Mean values of morphometric parameters for 93 basins across the eastern, central, and western zones, as well as the northern and southern sectors. Basins 1–37 are located in the western zone, basins 38–67 in the central zone, and basins 68–93 in the eastern zone. The number of basins is indicated by the letter N

Zone	N	AF	Bs	CI	HI	Smd	SL	Sd	Dd	Dd1	Df	N1/N
Western	37	12.77	1.8	1.54	0.5	1.19	317.5	1.26	5.1	2.82	12.02	0.72
Central	30	13.28	1.79	1.18	0.488	1.17	441.5	1.95	4.38	1.47	16.51	0.54
Eastern	26	13.63	2.02	1.24	0.496	1.10	309.4	1.09	2.96	1.45	10.21	0.69
Northern	51	13.36	2.18	1.36	0.49	1.17	372.3	—	4.28	3.10	14.04	0.48
Southern	42	13.1	1.61	1.31	0.49	1.15	312.1	—	3.11	1.54	11.08	0.65

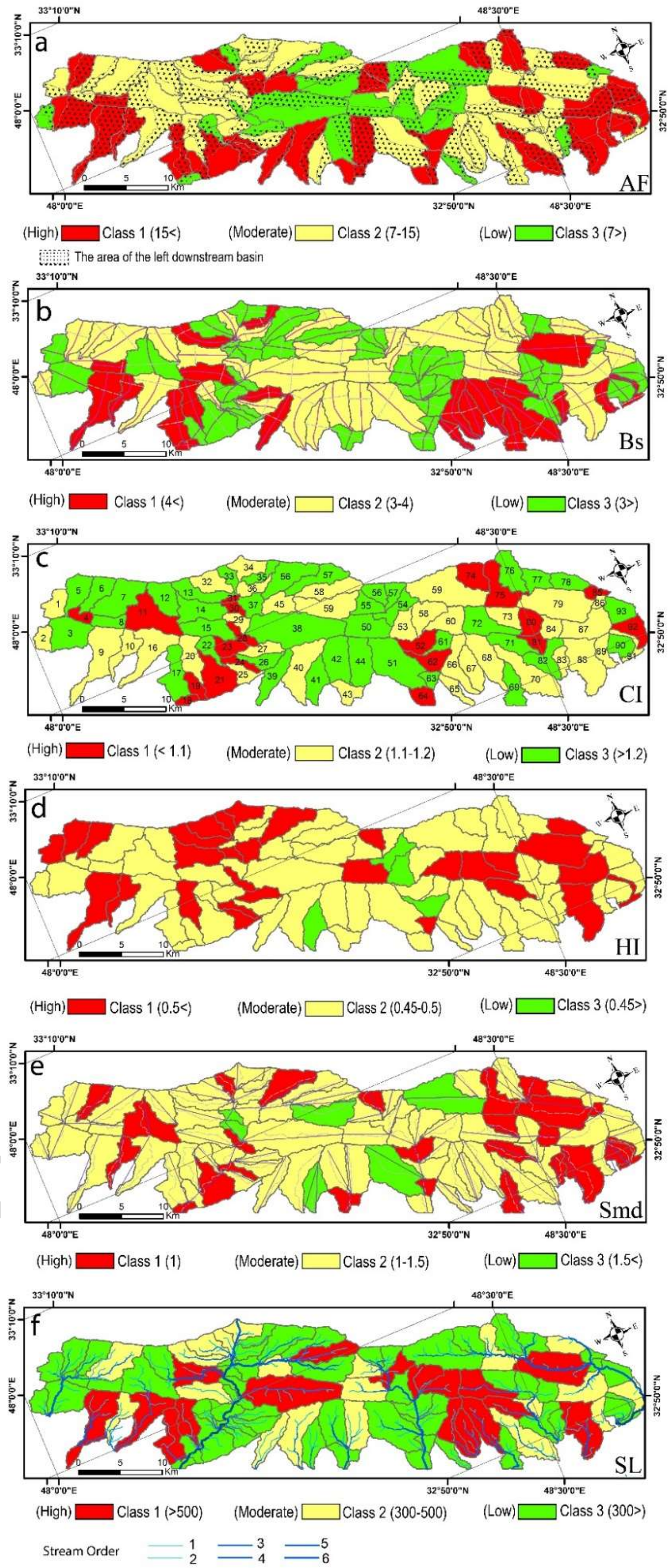

Figure 8. Zonation maps of the study area based on morphometric indices. (a) Asymmetry factor (AF). (b) Basin shape index (Bs). (c) Crescentness index (CI). (d) Hypsometric integral (HI). (e) Main drainage sinuosity (Smd). (f) Stream length-gradient index (SL). The drainage network is represented according to the Strahler's ordering system

The mean Bs values for the eastern, central, and western sectors are 2.02, 1.79, and 1.8, respectively, indicating that basins in the eastern sector are more elongated, while those in the central sector tend to be more circular. The average HI values are nearly identical across the three sectors. The highest mean CI occurs in the western sector (1.54), significantly exceeding the central sector (1.18, $p = 0.032$), but not the eastern sector (1.24, $p = 0.064$). Mean Smd values are highest in the western sector (1.19), followed by the central (1.17) and eastern (1.10) sectors. Based on AF values, the eastern basins show slightly higher mean asymmetry (13.63) than the western (12.77) and central (13.28) sectors. The mean SL values for the western, eastern, and central sectors are 317.5, 309.4, and 441.5, respectively, indicating that the central sector exhibits the highest SL values, while the western and eastern sectors show lower and relatively similar values.

Sd is greatest in the central sector (1.95), exceeding that of the eastern (1.09) and western (1.26) sectors. The drainage-network parameters—Dd, Dd1, and N1/N—are generally higher in the western (5.1, 2.82, and 0.72, respectively) compared to the central region (4.38, 1.47, and 0.54).

Table 1 also presents the average morphometric indices for the northern and southern flanks of the anticline. According to these results, the two flanks exhibit considerable differences. The northern limb shows higher drainage density (Dd = 4.28; Dd1 = 3.10) and drainage frequency (Df = 14.04), reflecting a more developed drainage network and more active lateral and vertical erosion. The lower proportion of first-order streams (N1/N = 0.48) indicates the presence of more high-order channels and a more evolved drainage system. The increased basin elongation (Bs = 2.18) may be influenced by structural trends or longitudinal slope conditions.

Conversely, the southern flank has lower drainage density (Dd = 3.11; Dd1 = 1.54) and reduced drainage frequency (Df = 11.08), suggesting less intense erosion or the presence of more resistant lithologies. The higher proportion of first-order streams (N1/N = 0.65) implies a younger drainage system that is still expanding laterally. Basins on the southern limb are also more compact (Bs = 1.61), which may correspond to a more symmetrical morphology or structural constraints.

Statistical analysis of six morphometric parameters across the three sectors of the Rit Anticline revealed significant spatial variations in four parameters. One-way ANOVA identified significant differences among the western, central, and eastern sectors in HI ($F = 5.946$, $p = 0.003$), CI ($F = 3.178$, $p = 0.046$), Smd ($F = 3.125$, $p = 0.048$), and SL ($F = 3.021$, $p = 0.036$), while AF ($F = 0.0718$, $p = 0.930$) and Bs ($F = 0.383$, $p = 0.682$) — the only two non-significant parameters — showed uniform distribution across all sectors (Table 2). Pairwise t-tests demonstrated that the western sector is morphometrically the most distinct (Table 2): compared to the central sector, it shows significantly lower SL (Mean_W = 317.5 vs. Mean_C = 441.5, $p = 0.028$), higher CI (1.54 vs. 1.18, $p = 0.032$), and higher HI (0.500 vs. 0.488, $p = 0.009$); compared to the eastern sector, it shows significantly higher HI (0.500 vs. 0.496, $p = 0.040$) and higher Smd (1.19 vs. 1.10, $p = 0.007$). No significant differences were identified between the central and eastern sectors in any of the six parameters (all $p > 0.05$). Pearson correlation analysis revealed four statistically significant relationships (Table 3): the strongest was a negative correlation between Bs and CI ($r = -0.411$, $p < 0.01$), while SL showed positive correlations with AF ($r = 0.204$, $p < 0.05$) and Bs ($r = 0.241$, $p < 0.05$), and a negative correlation with CI ($r = -0.222$, $p < 0.05$); all remaining parameter pairs were non-significant ($|r| \leq 0.13$).

Discussion

The present study investigates the influence of tectonic processes on the geomorphic characteristics, drainage systems, and channel networks of the Rit Anticline, located within the Simply Folded Belt of the Zagros orogen. Across the study area, a range of tectonically generated landforms is observed, reflecting the ongoing geodynamic activity of the region. These geomorphic features include triangular and trapezoidal facets, deep and narrow valleys, gorges, knickpoints, fault scarps, and steep mountain fronts. Their development is primarily associated with the activity of transverse–shear faults, thrusting, and syntectonic fold growth. The interaction of these structural elements with fault-related folding and river incision has reorganized the drainage network and produced distinctive tectonic geomorphological signatures. These features have evolved under the influence of the Balarud fault zone—part of the Mountain Front Fault—which forms the structural boundary between the Lorestan domain and the Dezful Embayment (Haj Ali Bigi et al., 2011).

River deflection is widely recognized as a key geomorphic indicator of lateral fold propagation (Ramsey et al., 2008; Song et al., 2011; Bahrami et al., 2020). This phenomenon is characterized by diverted river segments and fan-shaped drainage basins. For example, at Wheeler Ridge in California, drainage density systematically decreases from the fold core toward the fold tips, consistent with the direction of thrust propagation (Kleber et al., 2021). Within the Rit Anticline, geomorphic and structural evidence from different sectors highlights the strong imprint of neotectonic activity on drainage patterns and erosional processes. In the eastern sector, the presence of radial valleys, prominent fracturing, the transverse incision of the anticline by the Damdam River, steep mountain fronts, and triangular facets collectively indicate rapid uplift and an imbalance between erosion and tectonic forcing. Alluvial fans and landslides along the southern limb further point to slope instability driven by active tectonics.

The central sector is characterized by a continuous fold axis with gentle curvature, deep river gorges, and major incisions, reflecting competition between uplift and fluvial erosion. The preservation of the Zal River course through resistant formations and the development of young, fan-shaped drainage networks formed in response to steep escarpments and active faulting provide clear evidence of ongoing deformation. Headward erosion along the fold crest and the three wine-glass-shaped valleys developed within the footwall of the thrust fault demonstrate persistent neotectonic activity and its direct influence on drainage evolution.

Table 2. Results of pairwise Welch t-tests and one-way ANOVA for six morphometric parameters across the three sectors of the Rit Anticline (western, central, and eastern). T-tests assess pairwise differences between sectors; ANOVA tests for significant variation among all three sectors simultaneously

Parameter	***t*-test parameters**									**ANOVA parameters**	
	Western vs Central			**Western vs Eastern**			**Central vs Eastern**				
	T	**df**	**Sig (2-tailed)**	**T**	**df**	**Sig (2-tailed)**	**T**	**df**	**Sig (2-tailed)**	**F-statistic**	**p-value**
AF	0.226	52.999	0.821	-0.177	53.475	0.859	-0.358	53.282	0.721	0.0718	0.930
Bs	0.071	62.757	0.942	-0.751	53.914	0.455	-0.79	52.449	0.432	0.383	0.682
CI	2.199	50.978	0.032	1.8911	45.647	0.064	-0.683	52.702	0.4973	3.178	0.046
HI	2.747	31.839	0.009	2.1119	44.130	0.040	-1.833	35.878	0.075	5.946	0.003
Smd	0.491	58.715	0.625	2.7842	60.813	0.007	1.9156	50.557	0.061	3.125	0.048
SL	2.078	52.140	0.028	0.1055	58.610	0.916	1.2602	39.88	0.214	3.021	0.036

Table 3. Pearson's correlation matrix for morphometric parameters of studied drainage basins. ** Significant correlation at the 0.01 level. * Significant correlation at the 0.05 level

Parameter	AF	Bs	CI	HI	Smd	SL
AF	1					
Bs	-0.122	1				
CI	0.095	-0.411**	1			
HI	0.010	0.097	0.040	1		
Smd	-0.010	0.007	-0.129	-0.106	1	
SL	0.204*	0.241*	-0.222*	0.077	0.104	1

In the western part of the anticline, the interaction between fractures and the fold axis has produced transverse valleys, offset channels, and displaced layers—features that document coeval uplift and erosion. Triangular facets, curved and parallel drainage patterns, multiple erosional levels, alluvial fans, and axis deflection related to a left-lateral transverse–shear fault all reveal the high tectonic activity of this zone.

Morphometric indices also show significant contrasts among the western, central, and eastern sectors of the anticline. The central sector exhibits the highest drainage frequency (Df = 16.51) and the lowest ratio of first-order streams (N1/N = 0.54), indicating a mature, well-integrated drainage network with predominantly circular basins shaped by active lateral erosion. The western sector displays higher drainage density (Dd = 5.1; Dd1 = 2.82) and a greater proportion of first-order streams (N1/N = 0.72), reflecting a more actively evolving drainage system characterized by short and rapidly incising channels consistent with ongoing lateral fold propagation. The eastern sector, by contrast, shows the lowest drainage density and frequency (Dd = 2.96; Df = 10.21), along with elongated and asymmetric basins (Bs = 2.02; AF = 13.63), suggesting a less mature network with limited lateral expansion. Among the drainage parameters, Dd_1 most clearly separates the morphometric behavior of the sectors: a well-developed system in the central zone, a youthful and rapidly evolving network in the west, and a sparsely developed system in the east.

Morphometric variations between the northern and southern limbs of the anticline reflect different erosional regimes and evolutionary pathways. The northern limb exhibits higher drainage density (Dd and Dd1) and greater drainage frequency (Df), indicative of more vigorous erosion and a more advanced drainage network, possibly controlled by steeper slopes, abundant fractures, or mechanically weaker lithologies. The lower proportion of first-order streams (N1/N) shows that higher-order channels are well established, marking a mature network. The greater basin elongation (Bs) may reflect longitudinal fold growth or structural controls on basin shape. While average HI values across the three sectors appear similar at first glance (Western: 0.500, Central: 0.488, Eastern: 0.496), statistical analysis demonstrates that these differences are significant, with the western sector showing significantly higher HI than both the central and eastern sectors. Hypsometric curves are predominantly S-shaped across the anticline, consistent with the mature stage of landscape evolution (Strahler, 1952), reflecting dynamic equilibrium between tectonic uplift and erosion. The western sector shows significantly higher HI than the central sector (0.500 vs. 0.488, $p = 0.009$), consistent with more advanced fold propagation to the west. This westward increase in geomorphic maturity is consistent with a more advanced stage of drainage development in the western sector, where elevated CI values and greater main-channel sinuosity reflect prolonged interaction between fluvial erosion and tectonic forcing along the fold propagation front. The structural coherence of the anticline, reflected in the uniform distribution of AF and Bs across all sectors ($p > 0.05$), suggests that these HI differences arise from spatial heterogeneity in fold propagation rather than from differences in uplift rate or lithology alone.

Lithologies of moderate to low mechanical strength generally correspond to reduced values of HI, Bs, and AF, while promoting increases in CI, Smd, Sd, Dd, Dd1, and Df. The exposure of softer rocks enhances both lateral and vertical erosion. Figure 9 illustrates the percentage distribution of strong, intermediate, and weak lithologies across the three activity classes (1, 2, and 3) defined by the morphometric indices (AF, Bs, Smd, HI, SL, and CI). The occurrence of resistant lithologies within sectors characterized by relatively high tectonic activity suggests that uplift rates have locally exceeded erosion rates, maintaining the exposure of resistant carbonate units of the Asmari-Shahbazan Formation and Bangestan Group. Nevertheless, lithology still influences the geomorphic response of the landscape, as less resistant units promote drainage-network development and enhance erosion. Therefore, the observed geomorphic pattern reflects the combined effects of tectonic forcing and lithologic resistance, with tectonics acting as the primary control and lithology as a secondary modifier.

Complementary statistical analysis of six morphometric parameters across the three sectors provides quantitative support for the geomorphic patterns described above (Table 2). One-way ANOVA identified significant among-sector variation in four parameters: HI ($F = 5.946$, $p = 0.003$), SL ($F = 3.021$, $p = 0.036$), CI ($F = 3.178$, $p = 0.046$), and Smd ($F = 3.125$, $p = 0.048$), while AF and Bs showed no significant variation ($p > 0.05$), confirming the structural coherence of the anticline as a continuous fold. Pairwise t-tests further reveal that the western sector is morphometrically the most distinct: it differs significantly from the central sector in CI (Mean_W = 1.54 vs. Mean_C = 1.18, $p = 0.032$), HI (0.500 vs. 0.488, $p = 0.009$), and SL (Mean_W = 317.5 vs. Mean_C = 441.5, $p = 0.028$), and from the eastern sector in HI (0.500 vs. 0.496, $p = 0.040$) and Smd (1.19 vs. 1.10, $p = 0.007$). In contrast, no significant differences were identified between the central and eastern sectors in any parameter (all $p > 0.05$). The elevated SL values of the central sector likely reflect the interplay between lateral fold propagation and lithologic resistance. The dominant exposure of resistant Bangestan Group carbonates in the central sector — in contrast to the greater prevalence of softer formations such as the Amiran and Gurpi Formations in the western and eastern sectors — promotes vertical bedrock incision and steeper channel gradients. This lithologic contrast is itself consistent with the lateral propagation model, wherein the central sector, as the most structurally mature part of the fold, has experienced greater structural relief and differential erosional exposure compared to the younger propagating terminations. The elevated sinuosity of the western sector reflects the combined influence of softer formations and more advanced fold propagation — factors that are not mutually exclusive, as lateral propagation promotes exposure of less resistant lithologies, facilitating meander development. The lack of statistical differentiation between the central and eastern sectors supports the interpretation that lateral propagation to the east remains in a relatively earlier stage of development. Pearson correlation analysis (Table 3) further revealed that SL is positively correlated with both AF ($r = 0.204$, $p < 0.05$) and Bs ($r = 0.241$, $p < 0.05$), and negatively correlated with CI ($r = -0.222$, $p < 0.05$), indicating that steeper stream gradients are associated with larger, more elongated basins and are inversely related to crescent-shaped deformation — a pattern consistent with the dominance of vertical incision over lateral adjustment in structurally mature sectors. The strongest correlation in the dataset, between Bs and CI ($r = -0.411$, $p < 0.01$), reflects a geometric compensation between basin elongation and crescent-shaped deformation, suggesting differential fold curvature across the anticline.

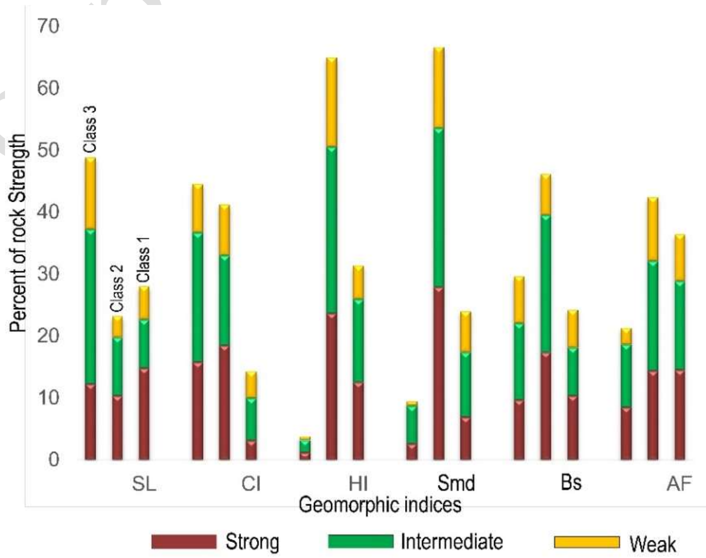

Figure 9. Percentage distribution of rock strength categories (strong, intermediate, and weak) across the three tectonic activity classes (Class 1: high, Class 2: moderate, Class 3: low) defined by CI, HI, Smd, Bs, AF, and SL for the 93 drainage basins of the Rit Anticline

Conclusion

The Rit Anticline, located in Lorestan Province within the Simply Folded Belt of the Zagros fold-and-thrust belt, is a fault-related fold whose drainage networks, basin morphometry, and geomorphic characteristics are strongly governed by active neotectonic forcing. Morphometric parameters — AF, HI, Bs, CI, Smd, and SL — were calculated for 93 drainage basins, and drainage-network indices (Dd, Dd1, Df, N1/N) were quantified across the western, central, and eastern sectors.

The central sector exhibits the highest SL values (mean = 441.5), consistent with vertical bedrock incision in the most structurally mature sector of the fold. The western sector represents the most morphometrically distinct zone, differing significantly from the central sector in three parameters (CI, HI, and SL) and from the eastern sector in two parameters (HI and Smd), collectively consistent with more advanced lateral fold propagation in this zone. The eastern sector shows no significant morphometric differentiation from the central sector, supporting the interpretation that lateral propagation to the east remains in an earlier stage of development. Differences between the northern and southern limbs reflect contrasting slope conditions, fracture intensities, and lithologic resistance that drive divergent erosional regimes. Geomorphic features including triangular facets, wine-glass–shaped valleys, transverse gorges, and alluvial fans further attest to the vigorous interplay between deformation and surface processes across the anticline.

Statistical analysis confirmed significant among-sector variation in HI, CI, Smd, and SL, while the uniform distribution of AF and Bs reflects the structural coherence of the anticline as a continuous fold. A strong negative correlation between Bs and CI ($r = -0.411$, $p < 0.01$) suggests geometric compensation between basin elongation and crescent-shaped deformation driven by differential fold curvature. Overall, the results demonstrate that the Rit Anticline is characterized by asymmetric bilateral lateral propagation — more morphometrically advanced to the west than to the east — confirming that the Rit Anticline represents an asymmetrically propagating fold system within the active geodynamic framework of the Zagros orogen.

Acknowledgments

The author thanks Professor Ali Kananian, Chief Editor of the Geopersia Journal for his editorial authority and constructive comments. I am grateful for the constructive comments of the anonymous reviewers, which helped to significantly improve the scientific content and presentation of the paper. The author would like to acknowledge the financial support of Lorestan University under grant number 14034045141405 for this research.

Conflicts of interest

The authors declare that there are no conflicts of interest regarding the publication of this paper. No financial or personal relationships exist that could have influenced the work reported in this manuscript.

Authors' contributions

Somaye Derikvand: Conceptualization, Methodology, Software, Validation, Formal Analysis, Investigation, Resources, Writing – Review and Editing, Supervision, Project Administration.
Fatane Rokrok: Investigation, Data Curation, Resources.

References

Agard, P., Omrani, J., Jolivet, L., Mouthereau, F., 2005. Convergence history across Zagros (Iran): constraints from collisional and earlier deformation. International Journal of Earth Sciences, 94: 401–419.

Agard, P., Omrani, J., Jolivet, L., Whitechurch, H., Vrielynck, B., Spakman, W., Wortel, R., 2011. Zagros orogeny: a subduction-dominated process. Geological Magazine, 148: 692–725.

Ahmadi, R., Ouali, J., Mercier, E., Mansy, J.L., 2006. The geomorphologic responses to hinge migration in the fault-related folds in the Southern Tunisian Atlas. Journal of Structural Geology, 28: 721–728.

Alavi, M., 1994. Tectonics of the Zagros orogenic belt of Iran: new data and interpretations. Tectonophysics, 229: 211–238.

Alipoor, R., Sadr, A.H., Nazari Dabir, H., Ghamarian, S., 2019. Assessment of relative active tectonic of the Garin Mountain using morphometric indices and fractal model analysis (Nahavand, west Iran). Quantitative Geomorphological Research, 7: 31-56.

Allen, M. B., Talebian, M., 2011. Structural variation along the Zagros and the nature of the Dezful Embayment. Geological Magazine, 148: 911–924.

Ashtraba, S., Alipour, R., Mohseni, H., 2019. Active tectonic evidences related to the Main Recent Fault in the Sarvabad region, NW Iran. Quaternary Journal of Iran, 5: 105-124.

Azor, A., Keller, E. A., Pinter, N., 2002. Geomorphic indicators of active fold growth: South Mountain-Oak Ridge anticline, Ventura basin, southern California. Geological Society of America Bulletin, 114(6), 745–753.

Bahrami, S., 2013. Analyzing the drainage system anomaly of Zagros basins: implications for active tectonics. Tectonophysics 608: 914–928.

Bahrami, S., Capolongo, D., Mofrad, M.R., 2020. Morphometry of drainage basins and stream networks as an indicator of active fold growth (Gorm anticline, Fars Province, Iran). Geomorphology, 355: 107086.

Bahrami, S., 2022. Analysis of confluence angle of drainages and its relation to morphometric properties of drainage basins in the Zagros Simply Folded Belt, Iran. Geomorphology, 400: 108091.

Bahrami, S., Stokes, M., 2023. Analyzing drainage basin orientation and its relationship to active fold growth: Handun anticline, Zagros, Iran. Geomorphology, 414: 108605.

Bahrami, S., Ehteshami-Moinabadi, M., Souri Tuyserkani, M., 2024. Quantitative evaluation of morphometric parameters of drainage system in the forelimb and backlimb of the Asmari Anticline, Zagros, Iran. Journal of Structural Geology, 184: 105151.

Bahroudi, A., Koyi, H.A., 2003. Effect of spatial distribution of Hormuz salt on deformation style in the Zagros fold and thrust belt: an analogue modelling approach. Journal of the Geological Society, 160: 719–733.

Bufe, A., Paola, C., Burbank, D.W., 2016. Fluvial beveling of topography controlled by lateral channel mobility and uplift rate. Nature Geoscience, 9: 706-710.

Burbank, D. W., Anderson, R. S., 2011. Tectonic geomorphology. John Wiley and Sons. 480 p.

Cox, R.T., 1994. Analysis of drainage-basin symmetry as a rapid technique to identify areas of possible Quaternary tilt-block tectonics: An example from the Mississippi Embayment. Geological Society of America Bulletin, 106: 571–581.

Deffontaines, B., Lee, C.T., Angelier, J., Carvalho, J., Rudant, J.P., Chen, R.F., 1992. Tectonic significance of drainage systems in the Taiwan Foothills. Geomorphology, 5: 199–211.

Delcaillau, B., Deffontaines, B., Angelier, J., Yu, M. S., 2006. Morphological records of active faulting and folding: Example of the Pakuashan anticline (Central Taiwan). Geomorphology, 76: 413–432.

Derikvand, S., Farahpour, M.M., 2020. Assessment of relative active tectonic of the Khorramabad Basin using morphometric indices and fractal model analysis (Lorestan, north-west Zagros belt). Quantitative Geomorphological Research, 9: 88-107.

Derikvand, S., 2023. Relative tectonic activity assessment and kinematic analysis of the north of Pole-Dokhtar, W Iran. Quantitative Geomorphological Research, 12(1), 241-259.

El Hamdouni, R., Irigaray, C., Fernández, T., Chacón, J., Keller, E.A., 2008. Assessment of relative active tectonics, southwest border of the Sierra Nevada (southern Spain). Geomorphology, 96: 150-173.

Faghih, A., Jamshidi, A., Nohegar, A., 2015. Geomorphic Assessment of Lateral Growth of Active Folds in the Fars Arc, Zagros Fold-Thrust Belt, Iran (Case Study: Herang and Kuh-e-Namaki

Anticlines). Scientific Quarterly Journal of Geosciences, 24: 133-142.
Falcon, N.L., 1974. Southern Iran: Zagros Mountains. In Mesozoic–Cenozoic Orogenic Belts: Data for Orogenic Studies. Geological Society, London, Special Publications, 4: 199–211.
Font, M., Amorese, D., Lagarde, J.L., 2010. DEM and GIS analysis of the stream gradient index to evaluate effects of tectonics: the Normandy intraplate area (NW France). Geomorphology, 119: 172-180.
Ghanadian, M., Faghih, A., Grasemann, B., Fard, I.A., Maleki, M., 2017. Analogue modeling of the role of multi-level decollement layers on the geometry of orogenic wedge: an application to the Zagros Fold–Thrust Belt, SW Iran. International Journal of Earth Sciences, 106: 2837-2853.
Hack, J.T., 1973. Stream-profile analysis and stream-gradient index. Journal of Research of the U. S. Geological Survey, 1: 421-429.
Haj Ali Bigi, A., Bahrami, S., Faghih, A., Fard, A., 2011. Structural evolution of the Zagros fold-thrust belt, Iran: Implications from the Lorestan and Dezful embayments. Journal of Asian Earth Sciences, 42: 1394–1406.
He, C., Cheng, Y., Rao, G., Yao, Q., Wang, L., 2019. Geomorphological signatures of the evolution of active normal faults along the Langshan Mountains, North China. Geomorphology, 334: 1–15.
Horton, R.E., 1932. Drainage-basin characteristics. Eos, Transactions American Geophysical Union, 13: 350–361.
Hubbard, J., Shaw, J.H., 2009. Uplift of the Longmen Shan and Tibetan plateau, and the 2008 Wenchuan (M = 7.9) earthquake. Nature, 458: 194–197.
Jamieson, S.S.R., Sinclair, H.D., Richardson, N.J., 2004. Tectonic forcing of longitudinal valleys in the Himalaya: Morphological analysis of the Ladakh Batholith, North India. Geomorphology, 58: 49–65.
Keller, E.A., Pinter, N., 2002. Active Tectonics: Earthquakes, Uplift, and Landscape, 2nd Ed. Prentice Hall, Upper Saddle River, N.J, p. 362.
Kleber, E.J., DeVecchio, D.E., Arrowsmith, J.R., Rittenour, T.M., 2021. Spatiotemporal rates of tectonic deformation and landscape evolution above a laterally propagating thrust fault: Wheeler Ridge anticline, California, USA. 2: 3395719.
Koshnaw, R.I., Kley, J., Schlunegger, F., 2024. The Miocene subsidence pattern of the NW Zagros foreland basin reflects the southeastward propagating tear of the Neotethys slab. Solid Earth, 15: 1365–1383.
Liffner, J.W., 2018. The sensitivity of catchment hypsometry and hypsometric integral to DEM resolution, DEM type and polynomial order. Geomorphology, 309: 112–122.
Lu, R., He, D., Xu, X., Wang, X., Tan, X., Wu, X., 2017. Seismotectonics of the 2016 M 6.2 Hutubi Earthquake: Implications for the 1906 M 7.7 Manas Earthquake in the Northern Tian Shan Belt, China. Seismological Research Letters, 89: 13–21.
Maleki, A., Yadegari, M., Bahrami, S., Alipoor, R., 2024. Morphometric evaluation of the drainage network of southwest Ilam watershedand its relationship with tectonics. Quantitative Geomorphological Research, 12: 30-49.
McClay, K.R., Whitehouse, P.S., Dooley, T., Richards, M., 2004. 3D evolution of fold and thrust belts formed by oblique convergence. Marine and Petroleum Geology, 21: 857–877.
McClusky, S., Reilinger, R., Mahmoud, S., Ben Sari, D., Tealeb, A., 2003. GPS constraints on Africa (Nubia) and Arabia plate motions. Geophysical Journal International, 155: 126–138.
Melosh, B. L., Keller, E. A., 2013. Effects of active folding and reverse faulting on stream channel evolution, Santa Barbara Fold Belt, California. Geomorphology, 186: 119–135.
Mirahadi, S.H., Izadikian, L., AliPoor, R., 2024. The Evaluation and efficiency of active tectonics in the northwest of the Sahneh using morphotectonic indicators. Quantitative Geomorphological Research, 13: 125-155.
Motiei, H., 1993. Stratigraphy of Zagros. Geological Survey of Iran Publication, Tehran, 536.
Pérez-Peña, J.V., García-Dueñas, V., López-Garrido, A., 2010. Active tectonics in the Sierra Nevada (Betic Cordillera, SE Spain): Insights from geomorphic indexes and drainage pattern analysis. Geomorphology, 118: 159–171.
Pirouvan, M., Shariat Jafari, H., 2013. Structural analysis and tectonic evolution of the Zagros fold-thrust belt, Iran. Journal of Structural Geology, 49: 1–16.
Ramasamy, S.M., Karthikeyan, S., Selvakumar, R., 2011. Drainage anomalies in South India—Indicators of active tectonics. Journal of the Geological Society of India, 78: 549–558.
Ramezani, N., Hakimi Asiabar, S., Dehbozorgy, M., Nozaem, R., Alianpour,H., 2023. Evaluation of the

tectonic activity of Biston-Kamiaran based on morphotectonic indices. Quantitative Geomorphological Research, 12: 101-119.
Ramírez-Herrera, M.T., 1998. Geomorphic assessment of active tectonics in the Acambay graben, Mexican Volcanic Belt. Earth Surface Processes and Landforms, 23: 317–332.
Ramkumar, M., Różycka, M., Stokes, M., 2019. Tectono-morphological evolution of the Cauvery, Vaigai, and Thamirabarani river basins, southern India: Insights from geomorphic indices and drainage patterns. Geological Journal, 54: 3451–3473.
Ramsey, L.A., Walker, R.T., Jackson, J., 2008. Fold evolution and drainage development in the Zagros Mountains of Fars Province, SE Iran. Basin Research, 20: 23–48.
Razavi Pash, M., Sarkarinejad, K., Motamedi, H., 2021. Structural relationship between subsurface oil fields in the northern Dezful Embayment: Qaleh Nar, Lower and Upper Balarud Anticlines. Journal of Petroleum Geology, 44: 375–396.
Sarkarinejad, K., Goftari, F., 2019. Thick-skinned and thin-skinned tectonics of the Zagros orogen, Iran: Constraints from structural, microstructural and kinematics analyses. Journal of Asian Earth Sciences, 170: 249–273.
Servati, M.R., Hosseinzadeh, M.M., Dehbozorgi, M., Nikpour, N., 2018. Geomorphological (morphotectonic) study of the middle part of the Kabirkuh anticline, Ilam: The area between Arisht Ridge and Emamzadeh Shah Mohammad Kuhneshin. Quantitative Geomorphological Research, 3: 104–123.
Sepehr, M., Honarmandnejad, M., 2012. Lithostratigraphy and tectonic evolution of the Zagros fold-thrust belt, southwest Iran. Journal of Asian Earth Sciences, 44: 1–16.
Simoni, A., Ghirotti, M., Berti, M., 2003. Geomorphological evidence of slope instability induced by tectonics in Northern Apennines (Italy). Geomorphology, 54: 21–43.
Singh, T., Jain, V., 2009. Tectonic constraints on watershed development on frontal ridges: Mohand Ridge, NW Himalaya, India. Geomorphology, 106: 231-241.
Song, S., Zhang, X., Yang, J., 2011. Drainage network evolution and its tectonic implications. Geomorphology, 128: 174–182.
Stokes, M., Mather, A., 2015. Engineering geology: An environmental approach. CRC Press.
Strahler, A.N., 1952. Hypsometric (area-altitude) analysis of erosional topography. Geological Society of America Bulletin, 63: 1117–1142.
Talebian, M., Jackson, J., 2002. Offset on the Main Recent Fault of NW Iran and implications for the late Cenozoic tectonics of the Arabia–Eurasia collision zone. Geophysical Journal International, 150: 422–439.
Talling, P.J., Sowter, M.J., 1999. Drainage network-scale characteristics of steep mountain catchments in the Karakoram Mountains. Basin Research, 11: 229–253.
Vernant, Ph., Nilforoushan, F., Hatzfeld, D., Abbassi, MR., Vigny, C., Masson, F., Nankali, H., Martinod, J., Ashtiani, A., Bayer, R., Tavakoli, F., 2004. Present-day crustal deformation and plate kinematics in the Middle East constrained by GPS measurements in Iran and northern Oman. Geophysical Journal International, 157: 381–398.
Wells, S.G., Bullard, T.F., Menges, C.M., Drake, P.G., Karas, P.A., Kelson, K.I., Wesling, J.R., 1988. Regional variations in tectonic geomorphology along a segmented convergent plate boundary pacific coast of Costa Rica. Geomorphology, 1: 239-265.
Xu, X., Wen, X., Yu, G., Chen, G., Klinger, Y., Hubbard, J., Shaw, J., 2009. Coseismic reverse-and oblique-slip surface faulting generated by the 2008 Mw 7.9 Wenchuan earthquake, China. Geology, 37: 515-518.
Yamani, M., Sharafi, S., 2011. Geometric parameters and their role in the temporal-spatial changes of river beds: A case study of the Harrod River, a tributary of the Karkheh River in Lorestan Province. Geography and Development Journal, 10: 35–48.
Zovoili, E., Konstantinidi, E., Koukouvelas, I.K., 2004. Tectonic geomorphology of escarpments: the cases of Kompotades and Nea Anchialos faults. Bulletin of the Geological Society of Greece, 36: 1716-1725.